energies

MDPI

Article

Research on GIS Partial Discharge Pattern Recognition Based on Transformer Algorithm

Chaofei Gao [1], Yanping Bai [2], Zan Wang [3], Lei Wang [1], Zhiyuan Wu [4] and Wei Wang [4,*]

1 School of Automation, Beijing Information Science & Technology University, Beijing 100192, China; gaocf@bistu.edu.cn (C.G.); 2025020452@bistu.edu.cn (L.W.)
2 Gansu Electric Transmission and Transformer Co., Ltd., Lanzhou 730050, China; gssbdbyp@163.com
3 State Grid Economic and Technological Research Institute Co., Ltd., Beijing 102209, China; wangzan22502@126.com
4 State Key Laboratory of Alternate Electrical Power System with Renewable Energy Sources, North China Electric Power University, Beijing 102206, China; wuzhiyuan@ncepu.edu.cn
* Correspondence: wwei@ncepu.edu.cn

Abstract

The Extrinsic Fiber Fabry–Perot Interferometer (EFPI) fiberoptic ultrasonic sensor can be used to detect partial discharge ultrasonic signals inside gas-insulated switchgear (GIS) and has various uses in pattern recognition research. Compared with traditional piezoelectric sensors, it offers both high sensitivity and strong resistance to interference. Based on this information, we construct four typical PD models (representing the tip, metal particle, suspension, and surface) in a GIS cavity filled with 0.4 MPa SF_6 gas, 0.6 MPa SF_6N_2 gas, and 0.5 MPa $C_4F_7NCO_2$ gas. We then use the EFPI sensor to detect PD ultrasonic signals, extract their waveform characteristics to form a database of characteristic parameters, and apply the Transformer algorithm. The detected signal offers outstanding pattern recognition when applied to GIS discharge samples in the laboratory, and the Transformer algorithm achieves a 100% recognition success rate, which is much higher than that of Support Vector Machine (SVM) machine learning algorithms.

Keywords: GIS; EFPI; pattern recognition; transformer algorithm

1. Introduction

When a partial discharge (PD) occurs in gas-insulated switchgear (GIS), it is often accompanied by electrical, acoustic, optical, and other physical phenomena. Partial discharge detection methods are categorized based on the physical event they detect, e.g., pulse current, UHF, ultrasound, and photons [1–3]. These detection methods have advantages and disadvantages. The pulse current method is the most direct and has the highest detection sensitivity, but it is vulnerable to electromagnetic noise interference at the laboratory site; thus, it must be utilized in a shielded room that is not conducive to online monitoring of electrical equipment. The UHF method is also highly sensitive, but it is expensive, requiring a large amount of equipment to collect high-frequency electromagnetic signals [4–7]. Ultrasonic signals inevitably attenuate during propagation in different media, and therefore the sensitivity of ultrasonic detection is lower than that of electrical methods. However, since ultrasonic detection relies on acoustic rather than electromagnetic signals, it is inherently immune to electromagnetic interference. It is also relatively inexpensive and can be used to locate discharge sources due to the good directivity of ultrasonic wave propagation.

Academic Editor: Claus Leth Bak

Received: 26 May 2026
Revised: 1 July 2026
Accepted: 9 July 2026
Published: 14 July 2026

Photon detection involves placing the detection sensor and insulating material in a dark environment with no obstacles between them, and thus has limited applicability [8–12].

Many scholars explored PD detection and pattern recognition in GIS [13–15]. In 2018, Tang Zhiguo and others conducted a study based on typical GIS defects. They obtained discharge data through experiments, used two common classifiers to identify the discharge based on a hierarchical recognition method, summarized incorrectly determined PD types, listed the causes of the errors that arose as a result of using the UHF method, and analyzed the similarities between discharge types [16]. In 2019, Ma Guoming and others studied ultrasonic detection methods using Michelson optical fiber interference, studied the influence of the mandrel size on sensor performance, and built an acoustic emission sensor performance test platform. The average sensitivity of the developed optical fiber ultrasonic sensor was 82.5 dB, with 0 dB = 1 $V/(ms^{-1})$, which was 18.7 dB higher than the Piezoelectric Transducer (PZT) sensor (R15a). The PD detection performance of an interferometric optical fiber ultrasonic sensor was tested using a 126 kV GIS. The results show that the resulting sensor could be used to detect PD ultrasonic signals from actual GIS equipment. Under the same ultrasonic signal excitation, the maximum response amplitude of the optical fiber sensor was 552% higher than that of PZT [17,18]. In 2017, Dong Ming et al. were the first to use silicon photomultiplier tubes to detect PD using optical signals [19]. They compared the detection results of traditional photomultiplier tubes and new silicon photomultiplier tubes on three typical GIS PD defects: guide rod spike, suspended discharge, and metal particles on an insulator surface. The detection sensitivity of the silicon photomultiplier tube was equivalent to that of a traditional vacuum photomultiplier tube. For various typical discharges, the detection sensitivity of a silicon photomultiplier tube was higher than that of a high-frequency current sensor [19,20].

Detection and pattern recognition of partial discharges in GIS are essential for assessing insulation condition. Ultrasonic detection offers strong immunity to electromagnetic interference, easy implementation, and low cost by capturing the ultrasonic signals generated by partial discharge events. Traditional piezoelectric sensors often have low detection sensitivity and poor electrical insulation. It is also difficult to obtain rich ultrasonic signal information when conducting tests through high-voltage electrical equipment shells, and it is impossible to identify the types of insulation defects that generate partial discharges. Therefore, to improve upon existing ultrasonic detection methods, we investigate partial discharge pattern recognition in GIS using an optical fiber EFPI ultrasonic sensor and the Transformer algorithm.

2. EFPI Ultrasonic Inspection System

In the EFPI sensing system, ultrasonic waves generated by PD are converted into optical signals at the sensor probe. The reflected optical signals are guided via a single-mode fiber to the optical fiber circulator for interference demodulation and subsequently transmitted to a photoelectric amplifier before they are observed on the oscilloscope. Through an analysis of the amplified signals following acousto-optic-electrical conversion, the characteristics of the insulation defects causing PD can be identified. A description of the operating principle of EFPI detection can be found in our previous publications [21,22].

In this paper, we use an EFPI ultrasonic sensor with a pressure balance structure to detect PDs. Due to the strong absorption effect of sulfur hexafluoride (SF_6) gas on ultrasound, the attenuation of the high-frequency components of ultrasound in SF_6 gas is more serious than that of the low-frequency components. The ultrasonic signal received by the EFPI sensor is mainly concentrated in the low-frequency band, so it is necessary to design the parameters of the EFPI sensor to improve its sensitivity and reduce its natural frequency. Therefore, we improve the sensitivity of the sensor by coating the inner surface

https://doi.org/10.3390/en19143316

of the membrane of the sensor probe and the end face of the optical fiber and redesign the size of the sensor probe to make the EFPI sensor more suitable for detecting the ultrasonic signals of partial discharges in SF6 gas. Photos of the coating of the sensor diaphragm and fiber are shown in Figure 1. SiO_2 and Ta_2O_5 are used for alternate coatings. The resulting ultrasonic waveform of the sensor in SF_6 is shown in Figure 2.

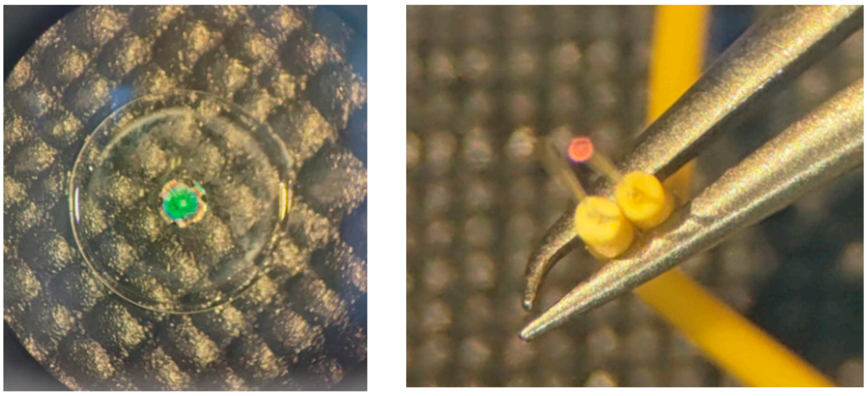

Figure 1. The coating of the sensor diaphragm and fiber.

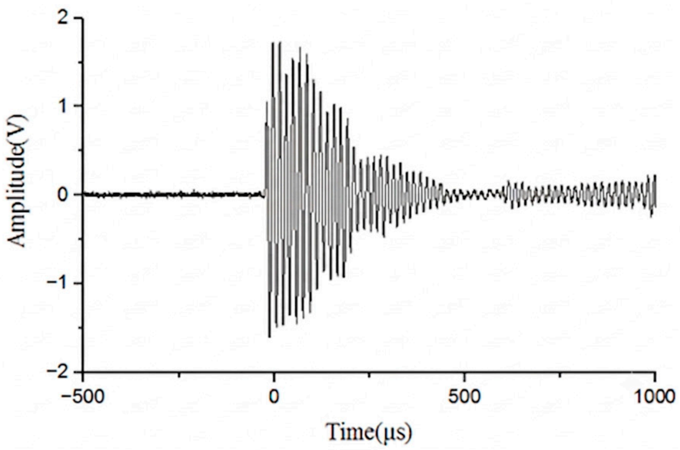

Figure 2. PD ultrasonic signal measured in SF6 by the new EFPI sensor.

3. Partial Discharge Ultrasonic Signal Detection

3.1. GIS Partial Discharge Detection Test Platform

Typical insulation defects in GIS include fixed protrusions, free metallic particles, poor conductor contact, surface cracks, and internal voids. In this study, four discharge models were created to simulate partial discharge phenomena associated with different insulation defects, namely tip discharge, metal particle discharge, suspended electrode discharge, and surface creeping discharge. Brass was selected as the conductive material for the defect models, while epoxy resin was used as the insulating material. The structural configurations of the defect models are illustrated in Figure 3. The experimental parameters of four PD models are provided in Table 1.

The discharge experiments were carried out in a GIS chamber filled with SF_6 gas at a pressure of 0.4 MPa. Under an AC voltage of approximately 18 kV, the four discharge models produced stable partial discharges and the corresponding ultrasonic signals could be successfully detected by the EFPI ultrasonic sensing system.

The experimental chamber employed in this work was a section of a 220 kV GIS manufactured by PINGGAO GROUP Co., Ltd. (Pingdingshan, China) The EFPI sensor installed inside the chamber was connected to the external detection system through an optical fiber feedthrough. FC/APC interfaces were adopted at both ends. The installation arrangement is shown in Figure 4.

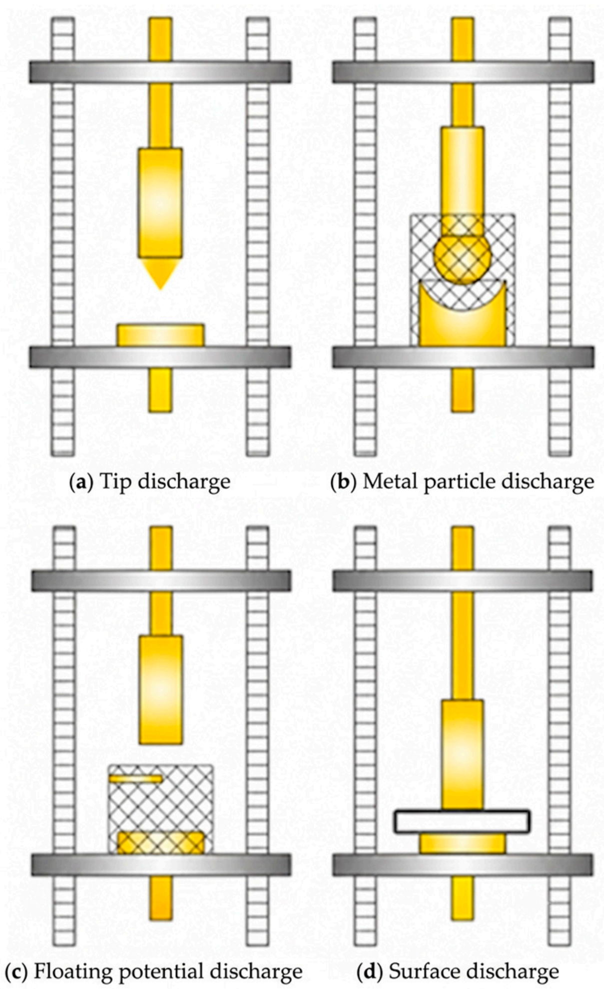

Figure 3. PD model of GIS insulation defects.

Table 1. Experimental parameters of four PD models.

Model	Material	Dimensions	Gap	Position
Tip discharge	Electrodes: copper metal; no additional insulating or particle components	Overall outer size: height 15 cm, base 10 cm × 10 cm. The upper electrode is a tapered cylindrical copper electrode and the lower electrode is a flat copper electrode	Adjustable gap between the tip of the upper electrode and the lower flat electrode	The upper and lower copper electrodes are vertically arranged coaxially, with the tip electrode on the top and the flat electrode at the bottom; the whole model is placed in the center of the test chamber
Metal particle discharge	Electrodes: copper metal; loose particles: aluminum spheres with diameters of 0.1 mm, 0.2 mm and 0.5 mm; insulating supports: polytetrafluoroethylene (PTFE)	Overall outer size: height 15 cm, base 10 cm × 10 cm. The lower copper electrode is supported by an insulating base and aluminum particles are placed in the concave insulating structure	Dynamic discharge gap formed by aluminum particles in the insulating region between upper and lower copper electrodes; the main electrode gap is adjustable	The upper and lower copper electrodes are vertically arranged coaxially. The PTFE insulating structure is fixed above the lower electrode, with aluminum spheres placed in the insulating cavity; the whole assembly is installed at the center of the test chamber

Table 1. *Cont.*

Model	Material	Dimensions	Gap	Position
Floating potential discharge	Main electrodes: copper metal; floating electrode: copper metal; encapsulating insulating material: polytetrafluoroethylene (PTFE)	Overall outer size: height 15 cm, base 10 cm × 10 cm. The floating metal electrode is wrapped and fixed by PTFE, with copper main electrodes at the top and bottom	Two fixed discharge gaps are formed between the floating electrode and the upper/lower main copper electrodes, respectively; gap sizes can be customized as required	The upper and lower main copper electrodes are vertically arranged coaxially. The PTFE-wrapped floating electrode is centrally placed between the two poles, and the entire model is located at the center of the test chamber
Surface discharge	Electrodes: copper metal; insulating dielectric plate: polytetrafluoroethylene (PTFE)	Overall outer size: height 15 cm, base 10 cm × 10 cm. The horizontal PTFE insulating plate is sandwiched between upper and lower copper electrodes	Discharge propagates along the upper and lower surfaces of the PTFE plate and fixed electrical gaps exist at the contact interfaces between electrodes and the insulating plate	The upper and lower copper electrodes are vertically arranged coaxially. The PTFE insulating plate is horizontally clamped between the two electrodes perpendicular to the electrode axis, and the whole structure is centrally mounted inside the test chamber

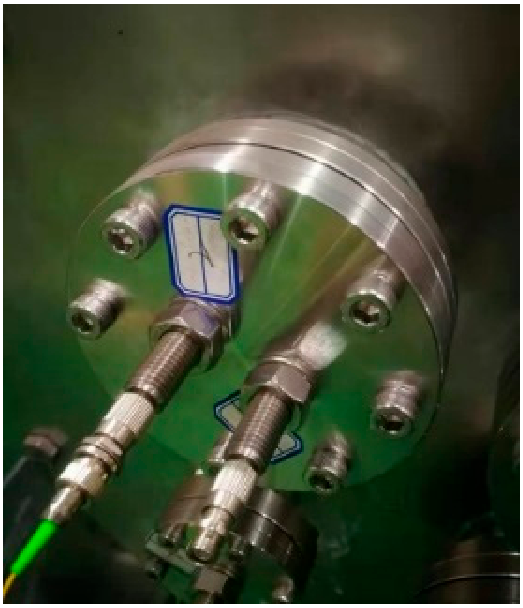

Figure 4. Installation method of fiber feedthrough.

3.2. Time-Domain Waveforms of Different Partial Discharge Types

Under an AC voltage of approximately 18 kV, all four typical insulation defect models were capable of generating stable partial discharges within the GIS experimental chamber. The gain of the photoelectric amplifier was set to 40 dB. The representative time-domain and frequency-domain characteristics of the four discharge models are presented in Figure 5.

The ultrasonic signals generated by different insulation defect models and detected by the EFPI sensors exhibit distinguishable overall waveform characteristics. Although certain discharge types—particularly floating potential discharge and surface discharge—exhibit partially overlapping features, the extracted ultrasonic characteristics remain sufficiently discriminative to support reliable feature extraction and subsequent pattern recognition.

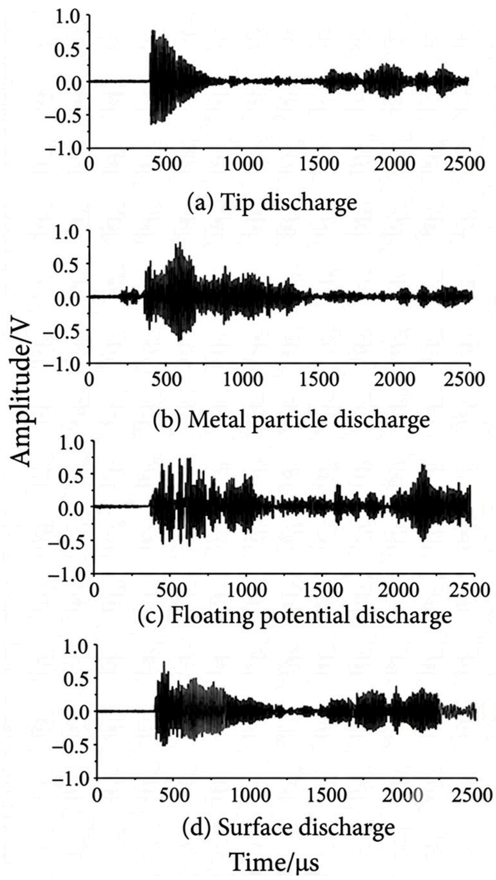

Figure 5. Ultrasonic signal waveforms of partial discharge models of different insulation defects.

4. GIS Partial Discharge Pattern Recognition Based on the Transformer Algorithm

4.1. Transformer Structure Composition

The Transformer model was initially applied in the field of Natural Language Processing (NLP) with great success. This has been attributed to its ability to train the entire text sequence in parallel. Due to its self-attention mechanism, it avoids the global dependency modeling of the input and output of the cyclic model structure. Transformer has the ability to process input sequences and dynamic capture of attention relations in parallel and has become a widely used sequence classification method. The general Transformer model has four important components: attention mechanism, multi-head attention mechanism, location coding, and a feedforward neural network structure [23–26].

4.1.1. Positional Encoding

Transformer uses global information. When utilizing sequence order information, positional encoding saves the relative or absolute position of the components in the sequence. The calculation formula is as follows:

$$\begin{cases} PE(pos, 2i) = \sin\left(\frac{pos}{10000^{\frac{2i}{d_{model}}}}\right) \\ PE(pos, 2i+1) = \cos\left(\frac{pos}{10000^{\frac{2i}{d_{model}}}}\right) \end{cases} \quad (1)$$

where i represents the dimension of the calculation object, and d_{model} is the dimension of the input vector. $2i$ represents an even dimension, whereas $2i + 1$ is indicative of an odd dimension.

4.1.2. Self-Attention Mechanism

To calculate the self-attention mechanism (SA), we begin by converting the input vector into three different vectors—query vector Q, key vector K, and value vector V—using linear matrix W^Q, W^K, and W^V. The self-attention is calculated as shown below:

$$\mathrm{Attention}(Q, K, V) = \mathrm{softmax}\left(\frac{Q \cdot K^T}{\sqrt{d_K}}\right) \cdot V \quad (2)$$

where d_k is the dimensionality of the Q and K vectors.

The attention calculation diagram is shown in Figure 6.

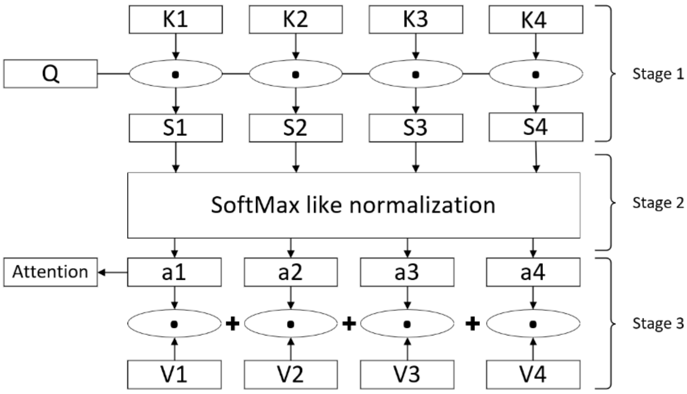

Figure 6. Attention calculation diagram.

4.1.3. Multi-Head Attention Mechanism

To simulate multiple paths in convolutional neural networks, multi-head attention (MHA) generates several groups of query vectors, key vectors, and value vectors from input slices and maps them into multiple subspaces to record the correlation between time sequences in parallel. The schematic diagram of the multiple-attention mechanism is shown in Figure 7.

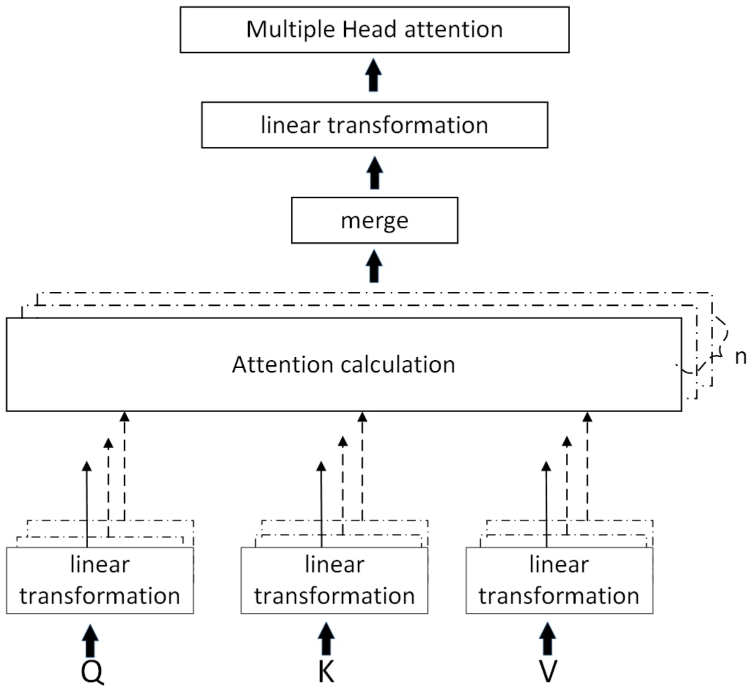

Figure 7. Schematic diagram of the multiple-attention mechanism.

4.1.4. Feedforward Neural Network

The feedforward operation of the Transformer model appears in the form of modules. When the task is complex and requires more information, additional data can be obtained by stacking modules. The modular design allows adjustments to be made in response to the model size during the building process, improving its flexibility.

4.2. Transformer Algorithm Flow

The main body of the Transformer framework adopts an "encoding–decoding" structure. A flowchart of the algorithm is shown in Figure 8. First, vector coding is performed on the input feature sequence, and the position of the feature quantity in the sequence is determined by adding it to the position coding. The weight is allocated multiple times through the full connection layer, and the query (Q), key (K), and value vectors (V) are obtained via linear mapping. The multi-head attention mechanism is used to calculate the correlation between the elements in the sequence, and the core feature fragments in the feature coding vector are adaptively selected. Feature codes are linearly mapped into vector space via a feedforward neural network. The decoder has a similar structure to the encoder. It inputs the target category sequence form and uses the mask category multi-head attention mechanism to actively query relevant feature information during each step while temporarily ignoring irrelevant details until the decoding operation is complete.

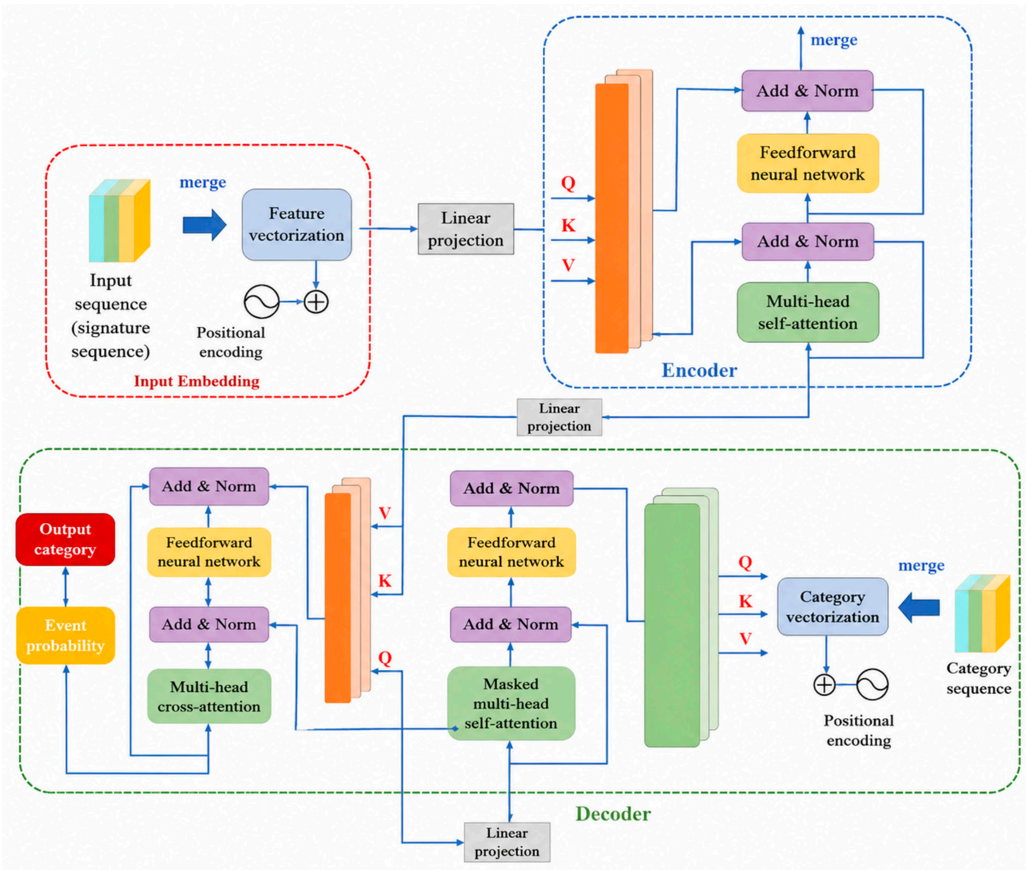

Figure 8. Transformer algorithm flowchart.

Unlike conventional pattern recognition methods, which rely on handcrafted feature extraction, the proposed Transformer-based approach uses the raw ultrasonic waveform as the model input. Firstly, the acquired signals are segmented into fixed-length waveform samples. Each waveform segment consists of 200 sampled amplitude values, which are treated as a one-dimensional single-channel sequence and directly fed into the Transformer model.

Instead of manually extracting statistical, frequency-domain, or time–frequency-domain features, the proposed method automatically learns discriminative feature representations through the embedding layer and the subsequent Transformer encoder during network training. This end-to-end learning strategy eliminates the need for handcrafted feature engineering and allows the model to learn representative features directly from the waveform data.

4.3. Comparison and Analysis of Identification Results

4.3.1. PD Pattern Recognition in SF_6 Gas

For the four insulation defect types, 300 PD ultrasonic signals (75 samples for each defect type) were collected, from which 300 groups of feature vectors were extracted. Subsequently, a characteristic parameter database was established and divided into training and testing sets with a ratio of 5:1. Figure 9 shows the identification and classification error results of test samples obtained using Transformer. Figure 10 shows the K-means clustering results obtained during the Transformer-based processing. The sum of squared errors (SSE) is used to evaluate clustering compactness, where lower values indicate better clustering performance.

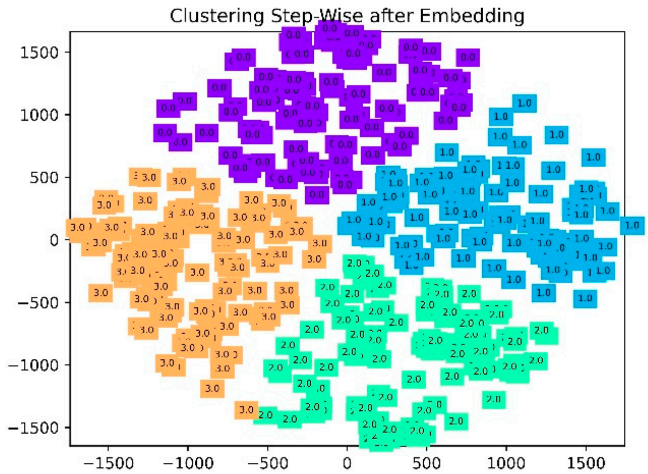

Figure 9. Pattern recognition and classification error results obtained using Transformer.

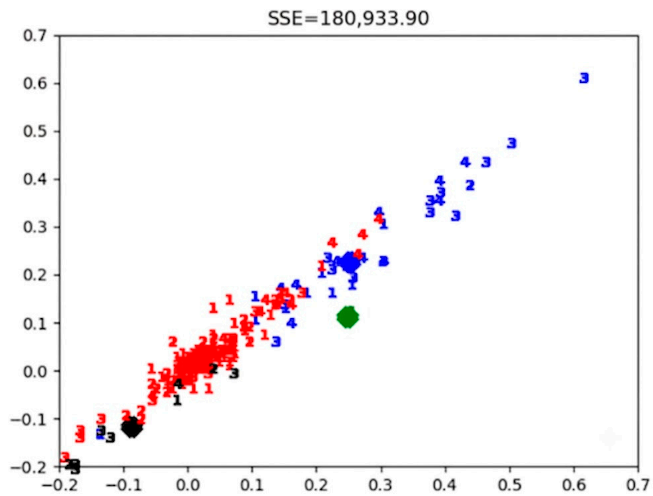

Figure 10. K-means clustering in Transformer algorithm processing.

The pattern recognition and classification error results are presented in Figure 9, while Table 1 summarizes the recognition accuracies of the Transformer algorithm for ultrasonic signals corresponding to different insulation defects. In our previous study, the recognition performance of the SVM algorithm was inferior to that of the Transformer-based approach [27].

As shown in Figure 9 and Table 2, the Transformer model achieved 100.0% recognition accuracy on the fixed testing dataset used in this study, demonstrating superior classification performance under the present experimental conditions. This result reflects the model's performance with regard to the specific testing subset adopted in this work and should not be interpreted as indicative of 100% generalization accuracy being achieved under all possible data partitions or operating conditions.

Table 2. Recognition accuracy of Transformer.

Discharge Type	Tip Discharge	Metal Particle Discharge	Floating Potential Discharge	Surface Discharge	Recognition Rate
Tip discharge	25				100%
Metal particle discharge		25			100%
Floating potential discharge			25		100%
Surface discharge				25	100%

4.3.2. PD Pattern Recognition of SF_6/N_2 Mixed Gases

As the proportion of SF_6 gas in the SF_6/N_2 gas mixture decreases, the insulation strength also decreases. The insulation level can be maintained by increasing the pressure of the gas mixture, but this also increases the pressure resistance requirements of the equipment. Relevant research shows that for a SF_6/N_2 gas mixture containing 25% SF_6 gas, increasing the gas pressure by 1.45 times ensures that the insulation strength of the gas remains unchanged. When SF_6 accounts for 30%, the gas pressure must be increased by 1.33 times to maintain the insulation level. The corresponding relationship between the specific mixing ratio and the gas pressure is shown in Table 3.

Table 3. Correspondence between mixing ratios and pressure.

SF_6 Mixing Ratio (%)	Pressure Increase Times	Proportion of SF_6 (%)
25	1.45	29
30	1.33	40
40	1.25	50
50	1.20	60

According to the results for the SVM recognition method shown in Tables 4 and 5, the recognition accuracy in the mixed insulation gas environment was greater than 84%, and it reached 90% in pure N_2 and in the 20% SF_6/80% N_2 mixed-gas environment. The pattern recognition of the Transformer algorithm achieved a success rate of up to 100%. As the SF_6 concentration in the SF_6/N_2 mixed gas decreased, the absorption of the ultrasonic signal by the insulation gas decreased simultaneously, with smaller attenuation of ultrasonic wave propagation in the GIS cavity; as such, more complete partial discharge information was retained.

https://doi.org/10.3390/en19143316

Table 4. SVM recognition accuracy with a 20%SF_6 80%N_2 gas mixture.

Discharge Type	Tip Discharge	Metal Particle Discharge	Floating Potential Discharge	Surface Discharge	Recognition Rate
Tip discharge	25				100%
Metal particle discharge	1	21	2	1	84%
Floating potential discharge			22	3	88%
Surface discharge			3	22	88%

Table 5. The 100%N_2 gas recognition accuracy of SVM.

Discharge Type	Tip Discharge	Metal Particle Discharge	Floating Potential Discharge	Surface Discharge	Recognition Rate
Tip discharge	25				100%
Metal particle discharge	2	21	1	1	84%
Floating potential discharge			23	2	92%
Surface discharge			3	22	88%

4.3.3. PD Pattern Recognition with C_4F_7N/CO_2 Mixed Gases

C_4F_7N is a new substitute for SF_6 gas that has attracted a great deal of attention in recent years. It has good insulation strength, stable chemical properties, and excellent environmental protection performance. It is also expensive and must be mixed with CO_2 gas as the insulating gas medium in power equipment. Existing research has demonstrated that the insulation strength of a C_4F_7N/CO_2 mixture with 20% C_4F_7N is equivalent to that of pure SF_6. A C_4F_7N/CO_2 mixture with 7–9% C_4F_7N also achieved the insulation strength of pure SF_6 when pressure was increased by a factor of 1.2–1.3.

The recognition accuracy of an 8%C_4F_7N/92%CO_2 mixed-gas environment at 0.6 MPa when SVM is used is shown in Table 6.

Table 6. Recognition accuracy of an 8%C_4F_7N/92%CO_2 mixed-gas environment at 0.6 MPa using SVM.

Discharge Type	Tip Discharge	Metal Particle Discharge	Floating Potential Discharge	Surface Discharge	Recognition Rate
Tip discharge	25				100%
Metal particle discharge	2	20	2	2	76%
Floating potential discharge			22	3	88%
Surface discharge			2	23	92%

The success rate of pattern recognition in 8%C_4F_7N/92%CO_2 mixed gas using the Transformer algorithm also reached 100%. Comparing Table 6 with Tables 4 and 5 revealed that the success rate of PD pattern recognition in different mixed gases using SVM was similar. Transformer achieved a much better performance.

5. Conclusions

In this paper, we presented an experimental device that allows us to simulate different partial discharges in GIS and four typical partial discharge models. We also described a way in which EFPI ultrasonic sensors can be used to measure the ultrasonic signals generated by the different types of partial discharges. In combination with waveform characteristics,

https://doi.org/10.3390/en19143316

we extracted feature parameters of the ultrasonic signal's single pulses and employed the Transformer algorithm to identify different fault types.

Our conclusions are as follows.

(1) The EFPI sensor in our design detects the discharge ultrasonic signal generated by four typical insulation defect models in GIS: tip, metal particle, suspension, and along-surface. The ultrasonic signal waveforms have prominent features that are conducive to subsequent feature parameter extraction and pattern recognition research.
(2) The Transformer algorithm has proven superior to the SVM algorithm in terms of its ability to correctly identify PD patterns, both in terms of recognition accuracy and in stability across gas mixtures.
(3) The proposed Transformer-based pattern recognition method achieved a recognition accuracy of 100% on the fixed testing dataset used in this study, demonstrating its effectiveness with regard to identifying typical GIS partial discharge types under the described laboratory conditions. The reported accuracy is specific to the experimental dataset employed in this work and does not imply universal performance under all practical conditions.

Future work will extend this comparative study by incorporating representative deep learning models, such as convolutional neural networks (CNNs) and long short-term memory (LSTM) networks, to further evaluate the advantages and limitations of the proposed Transformer-based method under identical experimental conditions.

Author Contributions: Methodology, C.G.; Software, C.G. and Z.W. (Zhiyuan Wu); Formal analysis, Z.W. (Zhiyuan Wu); Investigation, Z.W. (Zan Wang); Resources, C.G. and Z.W. (Zan Wang); Data curation, Y.B.; Writing—original draft, L.W.; Visualization, W.W.; Supervision, W.W.; Project administration, W.W. All authors have read and agreed to the published version of the manuscript.

Funding: This work was supported in part by the National Key Research and Development Program of China (Grant No. 2021YFB2400022).

Data Availability Statement: The original contributions presented in this study are included in the article. Further inquiries can be directed to the corresponding author.

Conflicts of Interest: Author Yanping Bai was employed by the company Gansu Electric Transmission and Transformer Co., Ltd.; Author Zan Wang was employed by the company State Grid Economic and Technological Research Institute Co., Ltd. The remaining authors declare that the research was conducted in the absence of any commercial or financial relationships that could be construed as a potential conflict of interest.

References

1. Zhou, H.; Ma, G.; Wang, Y.; Qin, W.; Jiang, J.; Yan, C.; Li, C. Optical sensing in condition monitoring of gas insulated apparatus: A review. *High Volt.* **2019**, *4*, 259–270. [CrossRef]
2. Ha, V.N.; Youn, Y.-W.; Choi, H.-S.; Nhung-Nguyen, H.; Kim, Y.-H. Self-Supervised Asynchronous Federated Learning for Diagnosing Partial Discharge in Gas-Insulated Switchgear. *Energies* **2025**, *18*, 3078. [CrossRef]
3. Wang, Z.; Liu, Z.; Qiao, L.; Qian, D.; Chen, Z.; Gao, C.; Wang, W. Research on Partial Discharge Pattern Recognition in GIS Based on EFPI Sensor. *J. Electr. Eng. Technol.* **2024**, *19*, 577–584.
4. Liu, Y.; Li, W.; Hua, X.; Liu, H.; Li, H.; Zhang, G.-J. A Swin transformer enhanced depthwise convolution with dynamic channel reweighting for partial discharge diagnosis in gas insulated switchgear. *Electr. Power Syst. Res.* **2025**, *248*, 111993. [CrossRef]
5. Ren, M.; Zhou, J.; Miao, J. Adopting spectral analysis in partial discharge fault diagnosis of GIS with a micro built-in optical sensor. *IEEE Trans. Power Deliv.* **2021**, *36*, 1237–1240. [CrossRef]
6. Darwish, A.; Refaat, S.S.; Abu-Rub, H.; Toliyat, H.A. PD signal propagation in GIS: Ultra-high frequency detection-based modeling. *IEEE Sens. J.* **2020**, *20*, 9417–9426. [CrossRef]
7. Han, X.; Li, J.; Zhang, L.; Pang, P.; Shen, S. A novel PD detection technique for use in GIS based on a combination of UHF and optical sensors. *IEEE Trans. Instrum. Meas.* **2019**, *68*, 2890–2897. [CrossRef]

8. Sun, S.; Sun, Y.; Xu, G.; Zhang, L.; Hu, Y.; Liu, P. Partial discharge pattern recognition of transformers based on the gray-level co-occurrence matrix of optimal parameters. *IEEE Access* **2021**, *9*, 102422–102432. [CrossRef]
9. Zhang, C.; Xu, Y.; Dong, M.; Burgos, R.; Ren, M.; Boroyevich, D. Design and assessment of external insulation for critical components in a medium voltage SiC-based converter via optical method. *IEEE Trans. Power Electron.* **2020**, *35*, 12887–12897. [CrossRef]
10. Li, J.; Zhang, X.; Han, X.; Yao, X. A partial discharge detection method for SF6 insulated inverted current transformers adopting inner shield case as UHF sensor. *IEEE Trans. Power Deliv.* **2018**, *33*, 3237–3239. [CrossRef]
11. Luo, H.; Liu, Y.; Guo, C.; Liang, Z. Optical detection and cluster analysis of metal-particle-triggered alternating current optical partial discharge in SF6. *Energies* **2025**, *18*, 1649. [CrossRef]
12. Fei, Z.; Li, Y.; Yang, S. Partial discharge pattern recognition based on an ensembled simple convolutional neural network and a quadratic support vector machine. *Energies* **2024**, *17*, 2443. [CrossRef]
13. Li, J.; Ma, S.; Jin, F.; Zhao, R.; Zhang, Q.; Xie, J. A study on partial discharge fault identification in GIS based on Swin Transformer-AFPN-LSTM architecture. *Information* **2025**, *16*, 110. [CrossRef]
14. Zhu, X.; Hu, C.; Yang, J.; Liu, Z.; Wang, Z.; Liu, Z.; Zang, Y. Acoustic identification method of partial discharge in GIS based on improved MFCC and DBO-RF. *Energies* **2025**, *18*, 1619. [CrossRef]
15. Song, H.; Dai, J.; Sheng, G.; Jiang, X. GIS partial discharge pattern recognition via deep convolutional neural network under complex data source. *IEEE Trans. Dielectr. Electr. Insul.* **2018**, *25*, 678–685. [CrossRef]
16. Tang, Z.; Tang, M.; Li, J.; Wang, J.; Wang, K.; Wu, C. Discussion on the resemblance of different partial discharges and accuracy of PD pattern recognition of GIS equipment. *High Volt. Eng.* **2018**, *44*, 2479–2485.
17. Ma, G.-M.; Shi, C.; Qin, W.-Q.; Li, Y.-B.; Zhou, H.-Y.; Li, C.-R. A non-intrusive electrical discharge localization method for gas insulated line based on phase-sensitive OTDR and Michelson interferometer. *IEEE Trans. Power Deliv.* **2019**, *34*, 1324–1331. [CrossRef]
18. Ma, G.-M.; Zhou, H.-Y.; Zhang, M.; Li, C.-R.; Yin, Y.; Wu, Y.-Y. A high sensitivity optical fiber sensor for GIS partial discharge detection. *IEEE Sens. J.* **2019**, *19*, 9235–9243. [CrossRef]
19. Ren, M.; Zhou, J.R.; Song, B.; Zhang, C.; Dong, M.; Albarracín, R. Towards optical partial discharge detection with micro silicon photomultipliers. *Sensors* **2017**, *17*, 2595. [CrossRef] [PubMed]
20. Ren, M.; Zhou, J.R.; Yang, S.J.; Zhuang, T.; Dong, M.; Albarracin, R. Optical partial discharge diagnosis in SF6 gas-insulated system with SiPM-based sensor array. *IEEE Sens. J.* **2018**, *18*, 5532–5540. [CrossRef]
21. Gao, C.; Yu, L.; Xu, Y.; Wang, W.; Wang, S.; Wang, P. Partial discharge localization inside transformer windings via fiber-optic acoustic sensor array. *IEEE Trans. Power Deliv.* **2019**, *34*, 1251–1260. [CrossRef]
22. Gao, C.; Wang, W.; Song, S.; Wang, S.; Yu, L.; Wang, Y. Localization of partial discharge in transformer oil using Fabry-Pérot optical fiber sensor array. *IEEE Trans. Dielectr. Electr. Insul.* **2018**, *25*, 2279–2286. [CrossRef]
23. Ramachandran, P.; Parmar, N.; Vaswani, A.; Bello, I.; Levskaya, A.; Shlens, J. Studying standalone self-attention in vision models. *arXiv* **2019**, arXiv:1906.05909.
24. Dosovitskiy, A.; Beyer, L.; Kolesnikov, A.; Weissenborn, D.; Zhai, X.; Unterthiner, T.; Dehghani, M.; Minderer, M.; Heigold, G.; Gelly, S.; et al. An image is worth 16×16 words: Transformers for image recognition at scale. *arXiv* **2021**, arXiv:2010.11929.
25. Zhao, H.; Jia, J.; Koltun, V. Exploring self-attention for image recognition. In Proceedings of the IEEE/CVF Conference on Computer Vision and Pattern Recognition (CVPR), Seattle, WA, USA, 13–19 June 2020; pp. 10073–10082.
26. Zhu, H.; Ke, W.; Li, D.; Liu, J.; Tian, L.; Shan, Y. Dual cross-attention learning for fine-grained visual categorization and object re-identification. In Proceedings of the IEEE/CVF Conference on Computer Vision and Pattern Recognition (CVPR), New Orleans, LA, USA, 19–24 June 2022; pp. 4682–4692.
27. Wang, Y.; Du, J.; Gao, C.; Song, S.; Wang, W. Study on partial discharge pattern recognition in oil based on F-P fiber optic ultrasonic sensor and probabilistic neural network. *High Volt. Appar.* **2018**, *54*, 152–158.